

## Article

# Investigation of the Influence of the Mixing Process on the Powder and Component Properties during Cyclic Reuse of a Polyamide 12 Sinter Material in Selective Laser Sintering

Tom Eggers \*  and Frank von Lacroix

Volkswagen AG Wolfsburg, Berliner Ring 2, 38440 Wolfsburg, Germany

\* Correspondence: tom.eggers1@volkswagen.de

**Abstract:** Selective laser sintering (SLS) with polymers is currently in transition to the production of functional components. Nevertheless, the potential to revolutionize conventional production processes is confronted by newly imposed requirements regarding reliability and reproducibility. To ensure that the requirements are fulfilled, the aging mechanisms occurring in polymers are compensated by recycling strategies, such as fraction-based mixing of a defined ratio of new with recycled powder. Although various mixing ratios for the reuse of the material in SLS have been investigated, there is insufficient knowledge of suitable mixing parameters for homogeneous and gentle mixing of the powder fractions. This work therefore focused on the influence of potentially suitable mixing parameters identified in a previous study on the ongoing powder and component properties in SLS using polyamide 12 and a constant refreshing rate. Regarding the powder properties, the intrinsic properties and density of the powders were investigated. Regarding the component properties, mechanical properties, sinter density, and surface quality were investigated. Decreases in the powder density and the component properties were measured by increasing the number of process cycles. Taking into account the determined powder and component properties, the selected mixing parameters enabled a homogeneous and gentle mixing of the powder fractions.

**Keywords:** additive manufacturing; selective laser sintering; polymers; powders; particles; powder density; interparticle forces; recycling; aging



**Citation:** Eggers, T.; von Lacroix, F. Investigation of the Influence of the Mixing Process on the Powder and Component Properties during Cyclic Reuse of a Polyamide 12 Sinter Material in Selective Laser Sintering. *Powders* **2023**, *2*, 75–96. <https://doi.org/10.3390/powders2010006>

Academic Editor: Paul F. Luckham

Received: 12 January 2023

Revised: 1 February 2023

Accepted: 2 February 2023

Published: 6 February 2023



**Copyright:** © 2023 by the authors. Licensee MDPI, Basel, Switzerland. This article is an open access article distributed under the terms and conditions of the Creative Commons Attribution (CC BY) license (<https://creativecommons.org/licenses/by/4.0/>).

## 1. Introduction

### 1.1. Technology of Selective Laser Sintering and Material Properties

Selective laser sintering (SLS) is a powder-based additive manufacturing process in which components are generated by applying layers and selectively solidifying primarily polymer materials by using heat [1–3]. Figure 1 shows the structure and subdivision of an SLS system. During the SLS process, the temperature of the powder bed should be kept constant between crystallization and melting temperature (sinter window) [1,4,5]. Due to the need for a sinter window for successful processing, only semi-crystalline thermoplastics are processed [1,5]. The following cooling process is controlled to avoid rapid recrystallization and to promote the coalescence of the molten powder [4–6]. Too-fast recrystallization of the materials leads to a reduced dimensional accuracy of the components due to the occurrence of deformations and curling effects [4,5]. Furthermore, the printing result is influenced by the choice of process parameters such as laser power, hatch distance, layer thickness, and scanning speed. Taking into account minimal distances between the components, the building platform can be fully utilized. The surrounding, non-solidified residual material can be reused [1,5]. In addition to the printing process, the complete SLS process also includes other steps such as pre-processing and post-processing [1–3,5].

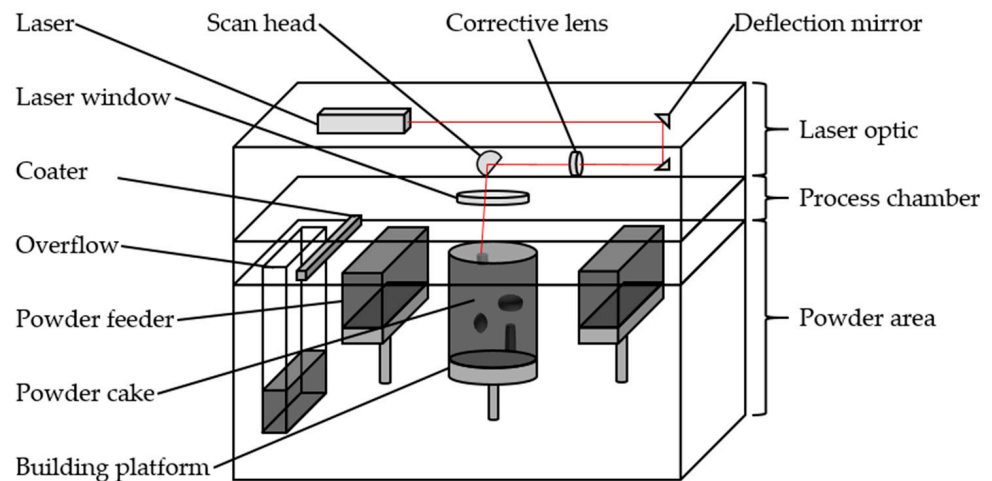


**Figure 1.** Design of an SLS system using the example of the Sintratec S2 laser sintering system from Sintratec AG. Subdivision of the SLS system into three areas.

The processability of the polymer in SLS is influenced by the material properties, which are divided into intrinsic and extrinsic properties [5,7,8]. The extrinsic properties include the particle shape, particle size, and particle size distribution (PSD) as well as the flowability of the powder particles [5,8]. In the case of a cohesive powder, there are interactions between the particles that influence the free flow of the powder particles [5,9]. The interparticle forces result from the presence of gravitational forces, mechanical interlocks, and van der Waals forces [5,9–11]. A spherical particle shape favors the flowability and applicability of the powder particles in the SLS process [5,7,8]. Mys et al. [12] list suitable particle shapes for use in SLS. Regarding the target component properties, SLS powders should allow a sufficient packing density of the applied layers [5,7,8]. In addition, environmental conditions such as temperature and humidity influence the flow behavior of the powder particles. The humidity absorbed by the powder leads to the formation of hydrogen bonds between the particles [9,13,14]. The intrinsic properties include the rheological, optical, and thermal properties [8]. For polymers used in SLS, an intermediate thermal range between the melting and crystallization points must be present. This sinter window is located in the metastable region of the undercooled melt and represents one of the main factors influencing the usability of, for example, polyamide 12 in terms of process suitability. A wide sinter window of the polymer favors easy process control and maintenance of temperatures in the building platform of the SLS system [5,7]. Furthermore, a low melting temperature of the polymer avoids the use of high energy densities, which result in a degradation of the material [1,5]. Regarding the rheological properties, a high melt viscosity reduces the flowability of the melt. In contrast, a low melt viscosity affects coalescence, so that the density and mechanical properties of the components are influenced [5,7,15,16]. Thus, a low melt viscosity of the polymer and a low surface tension of the melt prove to be suitable for a successful SLS process [5,7,8]. A high surface tension results in a decrease in the dimensional accuracy and surface quality of the components [17]. Furthermore, sufficient absorption of the laser beam by the polymer must be ensured [4]. Due to the necessity of a sinter window for the successful process flow in SLS, only semi-crystalline thermoplastics are processed. Polyamide 12 is the most commonly used material in SLS. However, other materials such as polyamide 11, thermoplastic elastomers, polypropylene, polyethylene, and polyetheretherketone are also used [1,4,5,18].

### 1.2. Aim of the Article

The powder material is exposed to various material aging processes, which are reflected as influences on the specific characteristics of the material [1,19–24]. These influences affect both the quality and reproducibility of the component properties and the process sta-

bility of the SLS process [1,5,6,19,20,25–27]. Recycling strategies [1,5,19,25–27] are used to compensate for these aging mechanisms. Therefore, the powder already used in the process is refreshed by adding new powder [1,5,19,25–27]. Gibson et al. [1] describe the fraction-based mixing of a defined ratio of new to recycled powder for cyclic reuse in SLS. With regards to polyamide 12, mixing ratios of 30% to 50% new powder with recycled powder are commonly used [1,5,19,22,26,28,29]. The heterogeneous properties of a powder mixture of new and recycled powder represent a significant cause of scattering [30]. Basically, the fraction-based mixing of a defined ratio of new with recycled powder must therefore be preceded by the selection of suitable mixing parameters. In this regard, Gibson et al. [1] aim to homogenize the powder fractions in a mixing process. In a previous part of this study [31], requirements for the mixing technology, the choice of mixing parameters, and the filling level of the mixing container are listed regarding the gentle and homogeneous mixing of the powder fractions. Furthermore, the study indicates suitable mixing parameters for the polyamide 12 sinter material and mixing technique used in this work. Although mixing ratios for the reuse of the material in SLS and suitable mixing parameters have already been investigated in previous studies, there is insufficient knowledge about the ongoing powder and component properties during cyclic use in SLS when using suitable mixing parameters. The aim of this work was therefore to investigate the influence of the identified mixing parameters on the powder and component properties in the course of ongoing processing in the SLS process at a constant refreshing rate. The focus of the investigation was on the thermal and rheological behavior, particle characteristics, and density of the powder, as well as on the mechanical properties, sinter density, and surface quality of the components. Therefore, the materials were cyclically reused using a constant refresh rate. For this purpose, standardized SLS print jobs were performed; the non-solidified, aged powder was collected, mixed with new powder using the previously mentioned mixing technology and mixing parameters [31], and added to the next print job as so-called printing powder. In addition, for each print job of a cycle, corresponding test specimens were generated and examined with regard to the focused component properties. Since polyamide is the most commonly used material in SLS [1,4,5,18] and the previously mentioned study [31] also refers to this material, polyamide 12 was also used in this study. The described method has not been used in previously mentioned studies [1,5,19,25–27]. This work revealed how cycling affects material and component properties so that abort criteria of cyclic use can be selected to achieve an acceptable component quality.

## 2. Materials and Methods

The storage of the materials and test specimens, as well as the application of the research methods, was carried out under controlled environmental conditions of 23 °C and 50% relative humidity. The materials and test specimens were stored airtight and protected from ultraviolet radiation.

### 2.1. Sinter Material

Polyamide 12 sinter material LUVOSINT PA12 9270 BK from the manufacturer Lehmann&Voss&Co.KG (Hamburg, Germany) was used. The material had a specific gravity of 1.02 g/cm<sup>3</sup> and a bulk density of 0.40 g/cm<sup>3</sup>. According to the data sheet, all unsolidified powder can be fully reused and no pre-drying is necessary. Furthermore, the sinter material required deagglomeration through a sieve with a mesh size of 250 µm before processing [32]. The choice of material was justified by the fact that polyamide 12 is the most commonly used sinter material in SLS [1,4,5,18].

### 2.2. Selective Laser Sintering Processing

The Sintratec S2 laser sintering system from the manufacturer Sintratec AG (Brugg, Switzerland) was used for SLS (Figure 1). The SLS system has a 10 W diode laser with a wavelength of 1064 nm. The building platform has a cylindrical design with an effective diameter of 130 mm and a maximum height of 360 mm. The powder bed surface was

heated up to a temperature of 175 °C for the sinter material at hand. No inert gas was used during the printing process. The used sinter material was printed with a layer height of 100 µm, a laser spot diameter of 145 µm, and a scanning speed during hatching of 3.85 m/s with a 90° layer offset. The boundary was printed at a scanning speed of 3.20 m/s. The used laser power was 10 W (100% laser power) and was in accordance with the specifications of the manufacturer of the SLS system. In this work, a standardized build job layout was used (Figure 2a).

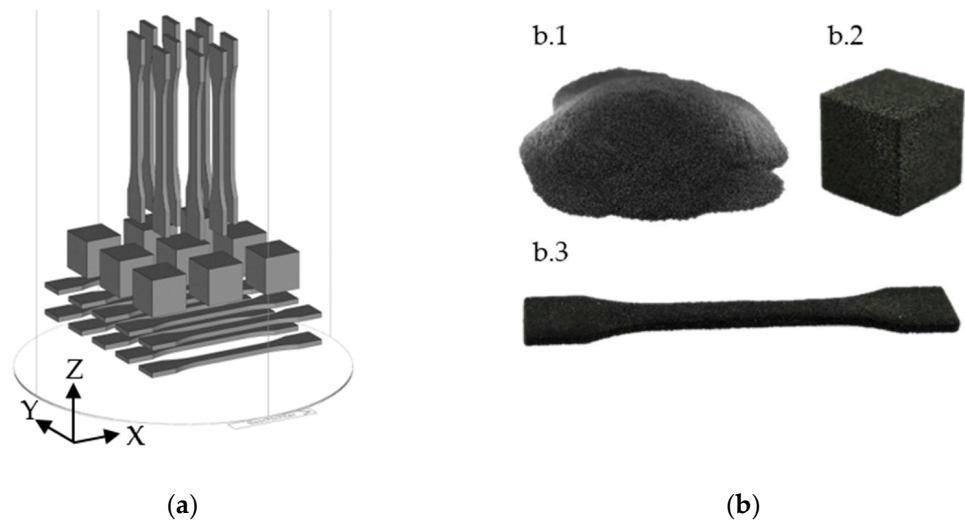


**Figure 2.** Illustration of the designed build job for the Sintratec S2 laser sintering system: (a) Orientation and placement of the test specimens in the building platform. The XYZ-specimens were oriented horizontally and the ZYX-specimens were oriented vertically. The coating direction was in the X-direction and the layer build-up in the Z-direction; (b) macroscopic images of sinter material and test specimen: (b.1) printing powder or aged powder; (b.2) cube; (b.3) tensile bar.

Before each printing process, the modules and tools of the SLS system were cleaned with a Hoover as well as dry cleaning wipes and isopropanol. For each printing process, 3.6 kg of powder was provided. The packing density was 3.3%. Table 1 lists the components and dimensions of the used specimens of the build job (Figure 2b). In order to investigate the powder and component properties during the cyclic reuse of the material, a total of five process cycles were considered. For each investigated process cycle, three printing processes were carried out and evaluated. The arithmetic mean value was formed over the three printing processes of each process cycle.

**Table 1.** Breakdown of the used specimens in the designed build job.

| Type            | Dimension        | Number | Usage                             |
|-----------------|------------------|--------|-----------------------------------|
| Tensile bar XYZ | 1BA <sup>1</sup> | 10     | Tensile test                      |
| Tensile bar ZYX | 1BA <sup>1</sup> | 10     | Tensile test                      |
| Cube            | 15 × 15 × 15 mm  | 9      | Sinter density, surface roughness |

<sup>1</sup> DIN EN ISO 527-2 [33].

Due to the glass transition temperature of polyamides, powder removal with a brush was carried out from a core temperature of the powder bed of 40 °C [1,5]. All non-solidified powder from the building platform, the feeders, and the overflow was extracted with a Hoover type NT 30/1 Te H from the manufacturer Kärcher (Winnenden, Germany) and collected via a cyclone separator type DLX MKII from the manufacturer Dust Commander (Sélestat, France). The collected powder was defined as recycled, aged powder and refreshed with 30 wt% new powder. The refresh rate was confirmed by various studies focusing on polyamide 12 [1,5,19,22,26,28,29], which identify mixing ratios of 30 to 50% new

powder with recycled powder. In addition, the refresh rate was in accordance with the specifications of the manufacturer of the SLS system. The powder mixture consisting of aged and new powder was called printing powder and was used for the next process cycle.

### 2.3. Sieving Technology

For the analysis of the powder characteristics and preparation of recycled powder, a vibration sieve machine of the type AS 200 basic from the manufacturer Retsch GmbH (Haan, Germany) was used. Test sieves according to DIN ISO 3310-1:2017-11 [34] with mesh sizes of 1000  $\mu\text{m}$ , 500  $\mu\text{m}$ , and 250  $\mu\text{m}$  were used and built up in decreasing mesh sizes. The excitation amplitude was set to 100 Hz and the sieving time to 15 min. Powder particles that did not pass the sieve tower after the defined time interval were not used for further investigations and cycles.

### 2.4. Mixing Technology

As a free-fall mixer, the tumbling mixer is a process that is gentle on the material to be mixed and ensures that the material is mixed as homogeneously as possible. There are no grinding bodies inside the mixing containers [35–41]. The powders were mixed using a Turbula T10B from the manufacturer WAB AG (Muttenz, Switzerland). A mixing time of 1 h and a mixing intensity of 15 rpm was used for mixing the powder fractions. These mixing parameters were in accordance with a previous part of this study [31] using the same sinter material. Mixing containers with a capacity of 5 L were used. A percentage filling level of 75% was applied and the mixing container was inserted into the mixer. This filling level was confirmed by investigations of Mwanja et al. [42] with similar polymer particles and Eggers et al. [31].

### 2.5. Particle Analysis

For the analysis of the particle shape and PSD by a dynamic image analysis according to ISO 13322-2:2021-12 [43], the particle analyzer type Camsizer XT from the manufacturer Retsch Technology GmbH was used. For the analysis of the particles, measurements with five million recorded particles in each case were carried out. As a result of the measurements, the sphericity and aspect ratio were available as mean values. In addition, the D10, D50, and D90 values, as well as the PSD, were outputs. The measurement did not provide for a standard deviation. Regarding the particle shape, the focus was on the sphericity and aspect ratio. The maximum value for sphericity and aspect ratio was 1 [5,44].

### 2.6. Scanning Electron Microscopy

The scanning electron microscopic (SEM) images of the sinter material were taken with a Tescan Mira 3 SEM system from the manufacturer Tescan GmbH (Dortmund, Germany). The microscope was operated with an acceleration voltage of 15 kV and the detection was carried out via secondary electrons. The specimens were first sputtered with gold for 40 s so that the particle surface was electrically conductive [45].

### 2.7. Classification of Powder Density

To determine the powder density, the bulk, and tap density were measured. The quotient of the tap and bulk density was named the Hausner factor [9,46,47]. As the Hausner factor only indicates the ratio of the two quantities, the Hausner factor was not used to describe the flow behavior of the powder particles. Spierings et al. [48] confirm this approach. Furthermore, studies [41,49–51] indicate a correlation between flowability and bulk density. The bulk density was determined according to DIN EN ISO 60:2000-01 [52] using a defined hopper from the manufacturer Landgraf Laborsysteme HLL GmbH (Langenhagen, Germany). A powder quantity of 110 mL to 120 mL was used for the measurement, which flowed through a hopper into a measuring cylinder. The bulk density was calculated via the ratio of the mass of the powder in the measuring cylinder and the volume of the measuring cylinder. The determination of the tap density was carried out with a tap volumeter from the manu-

facturer Landgraf Laborsysteme HLL GmbH according to the method described in DIN EN ISO 787-11:1995-10 [53]. The measuring cylinder was filled up to a measuring volume of  $200 \text{ mL} \pm 10 \text{ mL}$  with the powder. The powder was dried previously by a drying oven of the type TR 120 from the manufacturer Nabertherm GmbH (Lilienthal, Germany). After the compression process of 1250 revolutions of the camshaft, the volume after the last compression process was taken as the final volume. The tap density was calculated via the ratio of the mass of the powder in the measuring cylinder and the noted filling volume. The corresponding mass of the powder in the measuring cylinder was determined by a scale of the type EW 4200-2NM from KERN&Sohn GmbH (Balingen-Frommern, Germany). In order to achieve a higher statistical significance, three determinations of the bulk density and tap density of the powder were carried out and the arithmetic mean was calculated, contrary to the specifications in DIN EN ISO 60:2000-01 [52] and DIN EN ISO 787-11:1995-10 [53]. For the analysis of the recycled powder during cyclic reuse, this powder was first sieved with a vibration sieve machine.

### 2.8. Melt Flow Index Testing

The melt flow index testing of the powders was carried out with the Mflow measuring device from Zwick/Roell GmbH&Co.KG (Ulm, Germany) according to DIN EN ISO 1133-1:2012-03 [54]. A testing load of 2.16 kg at a temperature of  $190 \text{ }^\circ\text{C}$  and a filling quantity of 4 g was used to determine the melt flow rate (MFR). The powder was pre-dried at  $80 \text{ }^\circ\text{C}$  for 6 h. Drying was carried out using a TR 120 drying oven from Nabertherm GmbH. The test began by cleaning the nozzle with the cleaning tool and a cotton cloth. The measurement began at a piston position of 50 mm. Three sections were recorded at a measured length of 10 mm under an environmental temperature of  $23 \text{ }^\circ\text{C}$  and 50% relative humidity. The mass of each of the three sections was determined using an AB-100 scale from PCE Deutschland GmbH (Meschede, Germany). The MFR value resulted from the extruded mass within the defined interval and was given in g/10 min [54].

### 2.9. Differential Scanning Calometry Testing

Differential scanning calorimetry (DSC) was carried out to determine the sinter window using the DSC-822 measuring device from Mettler Toledo (Gießen, Germany). The measurements were carried out under a nitrogen atmosphere. A sample weight of  $10 \text{ mg} \pm 2 \text{ mg}$  was used for each measurement. In addition, heating and cooling cycles were carried out between 25 and  $230 \text{ }^\circ\text{C}$  at a rate of  $10 \text{ }^\circ\text{C}/\text{min}$ . The measurements were carried out according to DIN EN ISO 11357-1:2017-02 [55]. Both the melting and crystallization points, as well as the onset temperatures, were outputs. The measurement did not provide for a standard deviation. The sinter window was determined from the difference between the onset melting and onset crystallization temperatures [56]. The presence of a sinter window was necessary for the successful process flow of the SLS process [5].

### 2.10. Tensile Test

A Zwick/Roell Z100 tensile testing machine from Zwick/Roell GmbH&Co.KG was used to realize the tensile tests. The testing machine was equipped with a makroXtens mechanical extensometer, two wedge clamping jaws approved for up to a normal force of 10 kN, as well as an Xforce K load cell determined for the same load limit, and a testControl II control unit. The test specimens (Table 1) were dried in accordance with DIN EN ISO 16396-2:2017-07 [57] to reach a dry state at a temperature of  $60 \text{ }^\circ\text{C}$  and a vacuum of 70 mbar in a vacuum drying oven of type V0 400 from Memmert (Schwabach, Germany) for 95 h. The test specimens were then transferred to airtight containers together with silicate pellets for moisture absorption. The tensile test was carried out within five days after drying. The test specimens were stored packed at  $23 \text{ }^\circ\text{C}$  and 50% relative humidity for at least 24 h before testing. Thereafter, the test specimens were tested according to DIN EN ISO 527-1:2019-12 [58]. According to DIN EN ISO 16396-2:2017-07 [57], the tensile strength and elongation at break were recorded at a test speed of 50 mm/min, and Young's modulus

at a speed of 1 mm/min. Young's modulus was measured as secant modulus according to DIN EN ISO 527-1:2019-12 [58] in the elongation interval from 0.05% to 0.25%, and the specimens were exposed to a pre-load of 0.1 MPa at a test speed of 1 mm/min.

### 2.11. Sinter Density

Gravimetric density measurement was used to determine the sinter density [5]. The cubes (Table 1) were geometrically measured using the optical coordinate measuring system VL-550 from Keyence Corp. (Neu-Ilseburg, Germany). Table 2 lists the selected settings. Using strip light projections, specimen contours were captured with an accuracy of  $\pm 10 \mu\text{m}$ . The specimens to be analyzed were digitized and their volume was determined by assembling individual images. To digitize the specimens, they were recorded as tessellated half-shells and manually assembled into a closed body.

**Table 2.** Selected settings on the optical coordinate measuring system VL-550.

| Option           | Selected Settings |
|------------------|-------------------|
| Measuring method | Composition       |
| Measuring mode   | Manual            |
| Resolution       | Fine              |
| Brightness       | Auto (150)        |
| Measuring view   | Single view       |
| Rotation method  | Set angle         |
| Degree           | $360^\circ$       |
| Rotating segment | $60^\circ$        |

The mass of the specimens was determined using an AB-100 scale from PCE Deutschland GmbH. The quotient of mass and volume represented the sinter density.

### 2.12. Confocal Microscopy

The mobile confocal microscope MarSurf CM mobile from NanoFocus AG (Oberhausen, Germany) was used to determine the surface roughness and digitize the topography. The roughness measurements carried out were based on DIN EN ISO 4287:2010-07 [59] and DIN EN ISO 25178-1:2016-12 [60]. The generated data was transformed into roughness and flatness information using the  $\mu\text{soft}$  analysis extended software. The surface parameters  $S_a$  and  $S_z$  were used for the evaluation of the surface roughness due to the partially direction-dependent roughness of the surfaces [5,28,61,62]. For the analysis of the surface roughness, the cubes listed in Table 1 were used. To analyze the influence of the printing orientation on the surface roughness, the three main orientations [5,28] (upskin, sideskin, and downskin) were considered. Therefore, the measuring field was placed in the center of the cube faces. Table 3 lists the selected settings on the confocal microscope.

**Table 3.** Selected settings on the confocal microscope MarSurf CM mobile.

| Option             | Selected Settings                 |
|--------------------|-----------------------------------|
| Lens               | 800XS                             |
| Operating distance | 1 mm                              |
| Brightness         | 100%                              |
| Exposure           | 40 ms                             |
| Reinforcement      | 1.5 dB                            |
| Measuring field    | $2.1401 \times 2.1401 \text{ mm}$ |

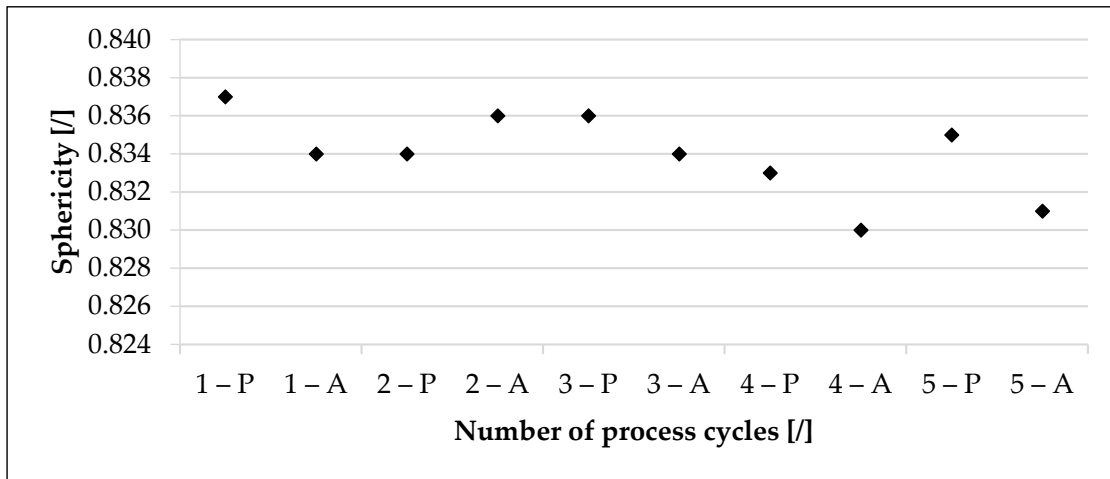
## 3. Results and Discussion

### 3.1. Influence of Cyclic Reuse on Powder Properties

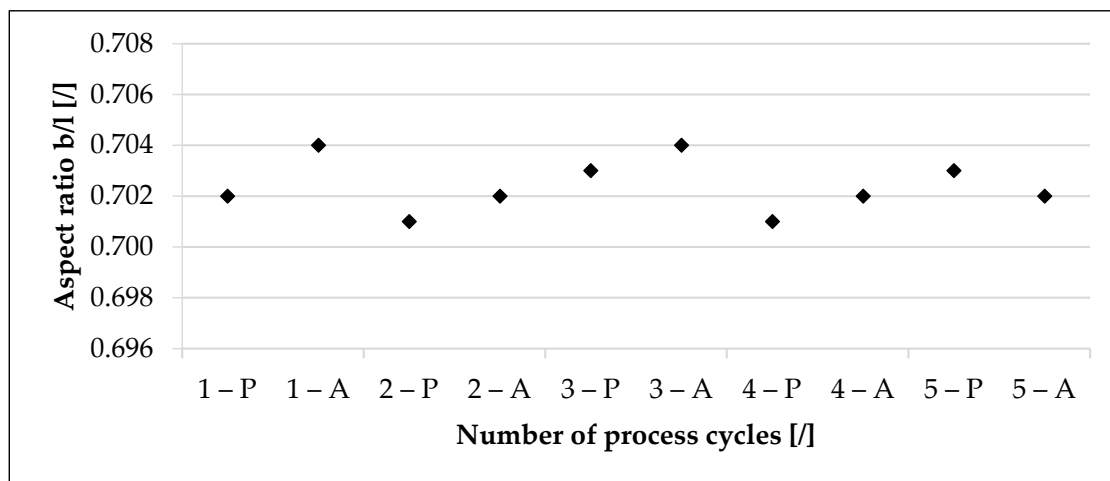
#### 3.1.1. Particle Shape and Particle Size Distribution

Figures 3 and 4 illustrate the influence of cyclic reuse of the sinter material on its sphericity and aspect ratio. The sphericity decreased, starting from the printing powder

of the first cycle (0.837) to the aged powder of the last cycle (0.831), by approx. 0.7%. In addition, the sphericity of the aged powder was lower than the sphericity of the printing powder at almost every process cycle. In contrast, the aspect ratio of the printing powder of the first cycle (0.702) to the aged powder of the last cycle (0.702) did not change in the measurable range. The maximum aspect ratio was 0.704 (1-A and 3-A) and the minimum aspect ratio was 0.701 (2-P and 4-P). Although there was a variation of approx. 0.2% between the process cycles, the aged powder of the last cycle had the same aspect ratio as the starting powder.

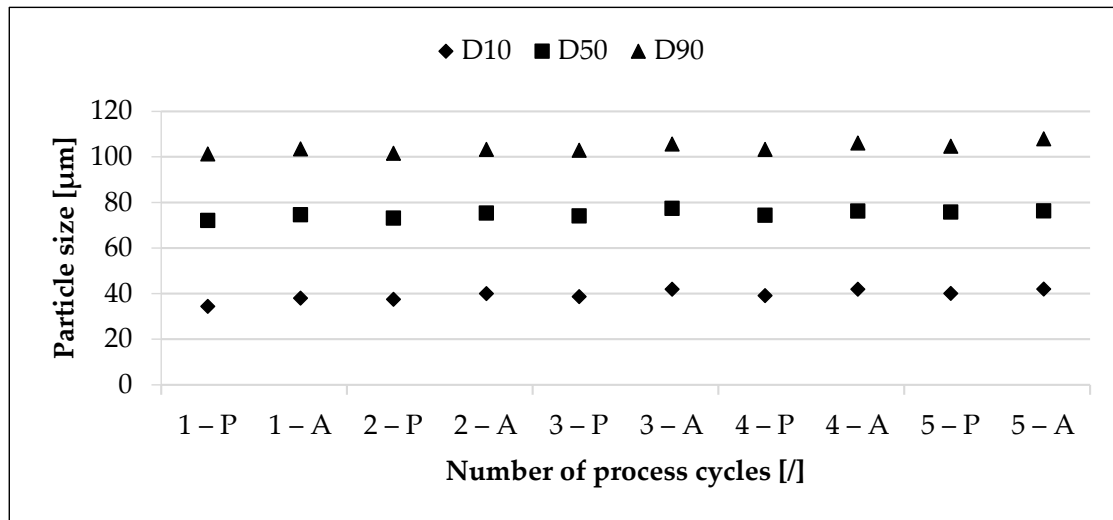


**Figure 3.** Influence of cyclic reuse on the sphericity of the used polyamide 12 sinter material. Five process cycles were considered. The printing powder (P) and the aged powder (A) were analyzed respectively. The refresh rate was 30 wt%. Determined with Camsizer XT.



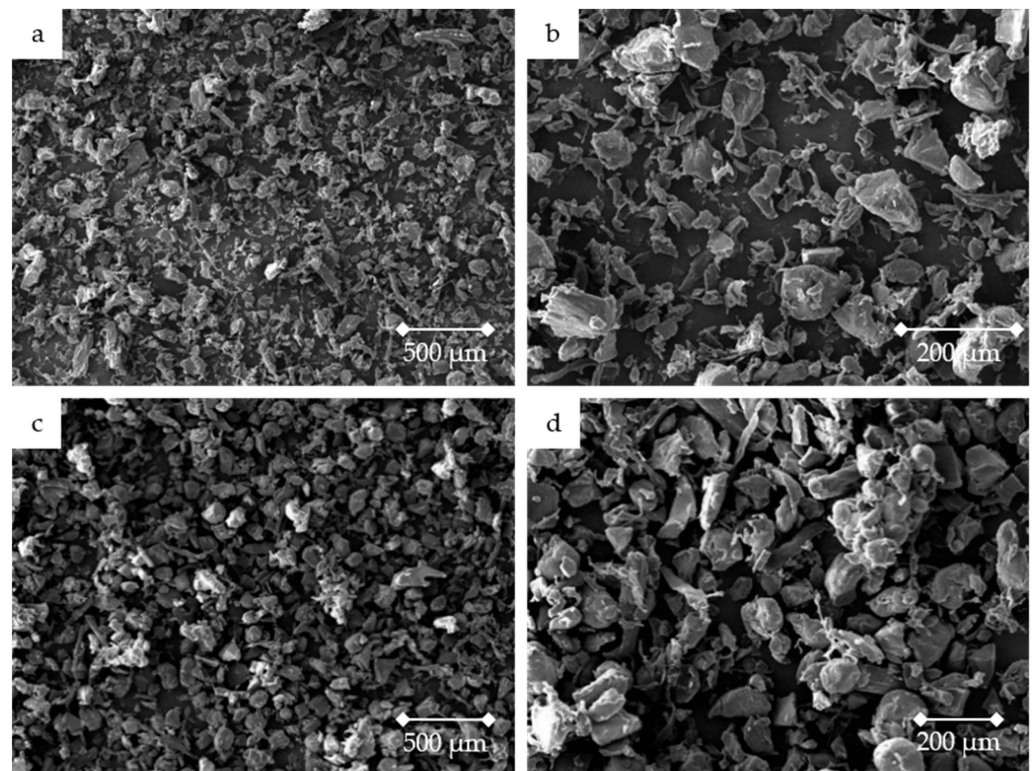
**Figure 4.** Influence of cyclic reuse on the aspect ratio of the used polyamide 12 sinter material. Five process cycles were considered. The printing powder (P) and the aged powder (A) were analyzed respectively. The refresh rate was 30 wt%. Determined with Camsizer XT.

Figure 5 illustrates that the particle size increased with the increasing number of process cycles. The base material showed a D10-value of 34.4  $\mu\text{m}$ , a D50-value of 72.1  $\mu\text{m}$ , and a D90-value of 101.3  $\mu\text{m}$ . Starting from the printing powder of the first cycle to the aged powder of the last cycle, the D10-value increased by approx. 22% (42.0  $\mu\text{m}$ ), the D50-value by approx. 5.8% (76.3  $\mu\text{m}$ ), and the D90-value by approx. 6.5% (107.9  $\mu\text{m}$ ). According to this, the fine particle fraction was especially reduced through the cyclic reuse and the PSD shifted towards higher particle sizes. Furthermore, the particle size of the aged powder after each process cycle was higher than that of the corresponding printing powder.



**Figure 5.** Influence of cyclic reuse on the characteristic values of the particle size distribution of the used polyamide 12 sinter material. Five process cycles were considered. The printing powder (P) and the aged powder (A) were analyzed respectively. The refresh rate was 30 wt%. Determined with Camsizer XT.

Figure 6 confirms the increase of the particle size during the cyclic reuse. Compared to the powder of the first process cycle, the powder after the fifth process cycle showed various particle agglomerates with a diameter of up to 250  $\mu\text{m}$ . In particular, small particles agglomerated to larger particles.



**Figure 6.** SEM images of the particles of the used polyamide 12 sinter material: (a,b) before the first process cycle at 46 $\times$  and 150 $\times$  magnification; (c,d) after the fifth process cycle at 46 $\times$  and 105 $\times$  magnification. Generated with Tescan Mira 3. Various particle agglomerates were visible in the powder after the fifth process cycle, with diameters up to 250  $\mu\text{m}$ . In particular, small particles agglomerated to larger particles.

### 3.1.2. Powder Density

Figures 7 and 8 illustrate the influence of cyclic reuse on the density of the powder. The bulk density and tap density of the aged powder decreased with the increasing number of process cycles. While the bulk density of the aged powder decreased by approx. 6.5% within five process cycles, the tap density of the powder decreased by approx. 4%.

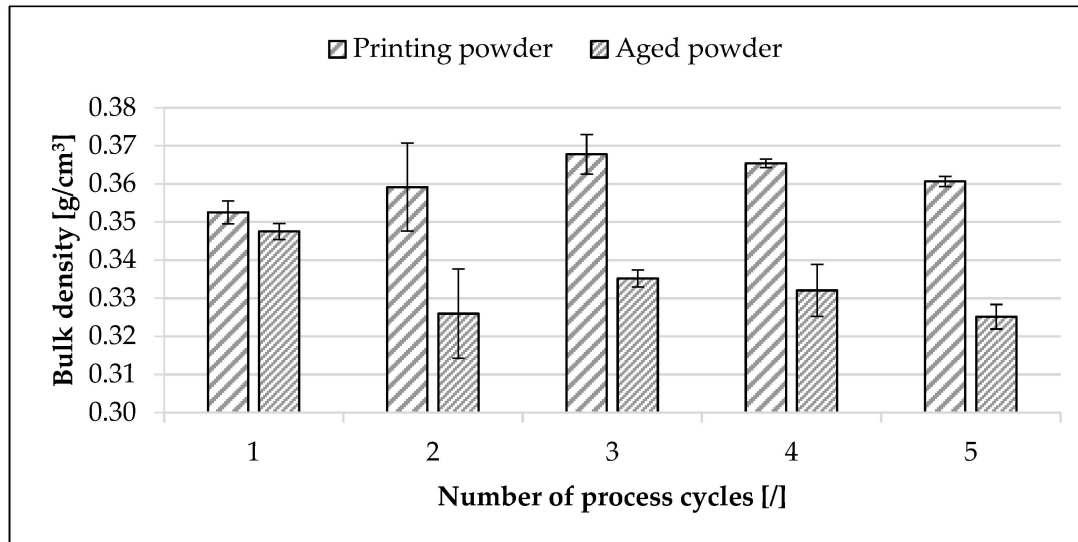


**Figure 7.** Influence of cyclic reuse on the bulk density of the used polyamide 12 sinter material. Five process cycles were considered. The printing powder and the aged powder were analyzed. The refresh rate was 30 wt%.

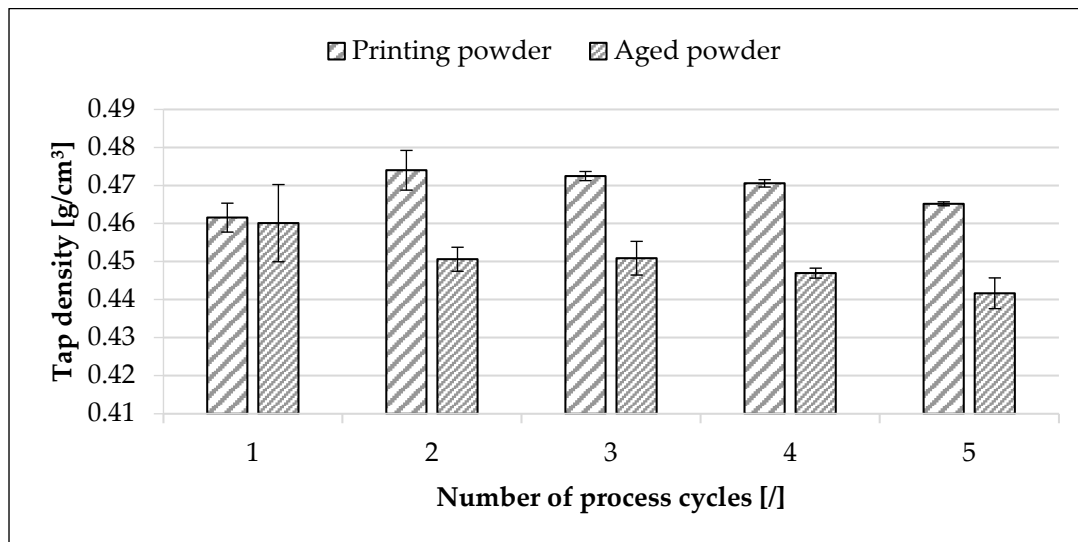


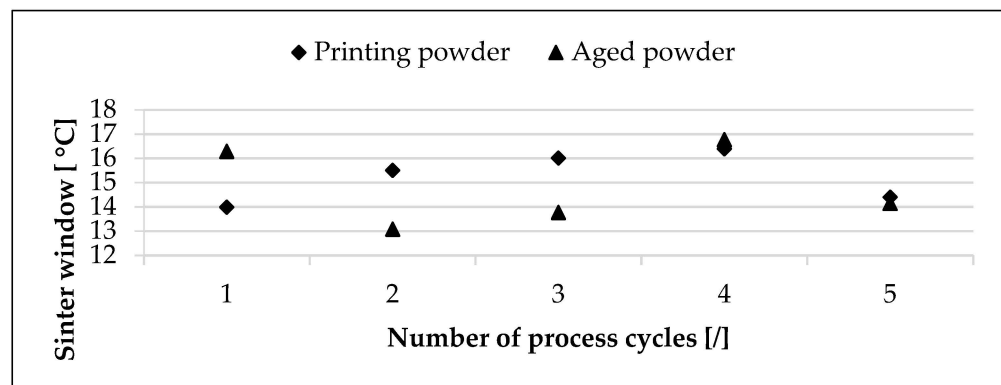
**Figure 8.** Influence of cyclic reuse on the tap density of the used polyamide 12 sinter material. Five process cycles were considered. The printing powder and the aged powder were analyzed. The refresh rate was 30 wt%.

In contrast, the density of the printing powder showed the opposite. The bulk density increased by approx. 2.3% and the tap density by approx. 0.8%. The density of the printing powder was higher than the density of the aged powder, regardless of the number of process cycles. In relation to the bulk density, the density of the printing powder in the first process cycle was approx. 1.5% higher than that of the aged powder. After five process cycles, the bulk density of the printing powder was approx. 10% higher than that of the

aged powder. Accordingly, the ratio of the bulk density and tap density of the printing powder to aged powder increased with cyclic reuse.

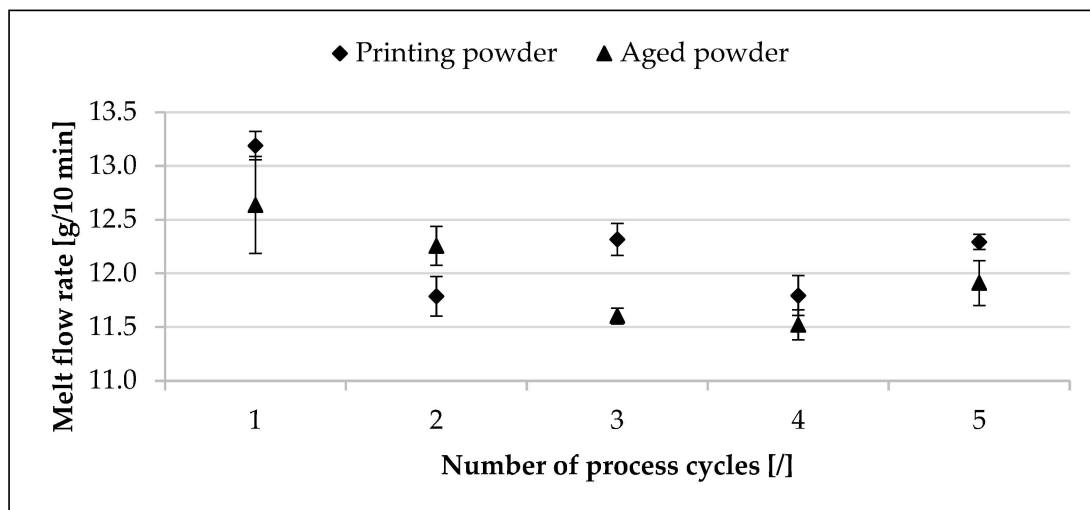
### 3.1.3. Thermal and Rheological Behavior

Figure 9 contains the results of the DSC analysis. The sinter window increased by approx. 16.5% in the first process cycle from printing powder (13.99 °C) to aged powder (16.29 °C). In the further cyclic reuse, the sinter window of the printing powder increased by approx. 16.4% up to the fourth process cycle. The sinter window then decreased by approx. 12.2% to a value of 14.4 °C. In contrast, the aged powder sunk temporarily below the sinter window temperature of the printing powder to a minimum value of 13.08 °C. Up to the fourth process cycle, the sinter window of the aged powder increased by approx. 3% to 16.77 °C. The sinter window then decreased by approx. 15.5% to 14.15 °C.



**Figure 9.** Influence of cyclic reuse on the sinter window of the used polyamide 12 sinter material. The sinter window was determined from the difference between onset melting and onset crystallization temperature. Five process cycles were considered. The printing powder and the aged powder were analyzed. The refresh rate was 30 wt%.

Figure 10 illustrates the results of the melt flow index measurement. Starting with the printing powder in the first process cycle (13.19 g/10 min), the MFR value decreased by approx. 9.7% until the aged powder of the last process cycle. The MFR value decreased by approx. 12.5% until the fourth process cycle and increased up to the aged powder of the last process cycle by approx. 3.4% to a MFR value of 11.91 g/10 min.



**Figure 10.** Influence of cyclic reuse on the melt flow rate of the used polyamide 12 sinter material. Five process cycles were considered. The printing powder and the aged powder were analyzed. The refresh rate was 30 wt%.

### 3.1.4. Discussion of the Results of the Studies on Powder Properties

Contrary to previous studies [16,63], Figures 3 and 4 indicate that the shape factors of the particles only marginally decreased or stagnated. Although the SEM images shown in Figure 6 illustrate an increasingly jagged and deformed particle shape, this observation was not found in the analysis of the shape factors. A possible change in the shape factors could be overlaid through the formation of agglomerates and the adhesion of small particles to large particles, so this was not apparent. In addition, the refresh rate of 30 wt% could have been the reason for the low decrease or stagnation of the form factors. This suggests that the refresh rate was high enough to maintain the form factors. Furthermore, the number of investigated process cycles might not have been high enough to indicate measurable influences on the form factors. The increase in sphericity from the corresponding aged powder to the printing powder was possibly due to the refreshment. Although the sphericity of the printing powder increased again, the level of the base material was no longer reached.

The agglomeration of the particle could be the reason for the increase in particle size (see Figure 5) with an increasing number of process cycles. In particular, the fine particles were lost and the particle size increased. The extrinsic causes of aging due to the cyclic reuse of the polymer were confirmed by various studies [64–67]. The loss of fine particles and the increase in particle size were due to the formation of agglomerates as a result of interparticle forces and the sintering of small particles. The SEM images shown in Figure 6 confirm this assumption, as agglomerates were formed after only a few process cycles and the fine particles adhered to large particles or joined together to form larger particles. In addition, electrostatic forces between the particles are also conceivable, leading to the formation of agglomerates during the ongoing use of the material [17,68]. Even though these forces were not investigated in this work. Furthermore, there is the possibility that fine particles form a particle cloud as a result of the cyclic reuse during the preparation and processing of the powder in the SLS system, which is deposited on any neighboring surfaces [1]. Although this could not be proven within the scope of the investigation, this assumption cannot be completely excluded. Especially in the pre-processing and post-processing of particle clouds form, which are preferentially extracted and captured.

The deformation and damage of the particles recorded in Figure 6, together with the increase in particle size shown in Figure 5, affected the density of the powder in the cyclic reuse (Figures 7 and 8). The arithmetic mean values of bulk and tap density shown in Figures 7 and 8 had low variation coefficients of less than 5%. Furthermore, the printing powder had at least a stagnation of the bulk and tap density independent of the number of process cycles. Therefore, the selected mixing parameters seemed to be suitable regarding the homogeneous mixing of the powder fractions. The decrease in bulk and tap density of the aged powder with the increasing number of process cycles has been confirmed by various studies [63–65,67,69,70], which note a direct influence of particle shape, particle size, and PSD on the flowability of powders particles. The increasing ratio of the bulk and tap density of printing powder to aged powder with the increasing number of process cycles was due to both the refreshment and the increasing influence on the already recycled fractions.

Contrary to previous studies [64,69,71–76], no measurable increase in the sinter window as a result of cyclic reuse was recorded in the DSC analysis (Figure 9). Only in the first process cycle from the printing powder to the aged powder could this influence be determined. However, the sinter window scattered within the investigation, so no clear tendency was identifiable. The reason for this was possibly the overlapping of the material aging due to the constant refreshing with new powder as well as the number of investigated process cycles, which represents an insufficient aging period.

The results of the melt index measurement (Figure 10) were not in accordance with previous studies [6,19,22,64,65,70–75,77–86] concerning the influence of cyclic reuse on melt viscosity. The studies predominantly found an increase in melt viscosity with increasing cyclic use. The reason for the deviating results could be overlapping effects due to the constant refreshment with new powder as well as a too-low number of investigated process

cycles. Mixing the non-solidified powder fractions from the building platform, feeder, and overflow superimposes the change in melt viscosity [22,85]. The result of the MFR measurement, as well as the low variation coefficients of less than 5%, indicate that the refreshment led to a maintained melt viscosity and that the selected mixing parameters were suitable for homogeneous mixing.

### 3.2. Influence of Cyclic Reuse on Component Properties

#### 3.2.1. Mechanical Properties

Figure 11 illustrates the influence of cyclic reuse on Young's modulus. While Young's modulus of the XYZ-specimens increased by approx. 0.12% during reuse, Young's modulus of the ZYX-specimens increased by approx. 11.5% from the first to the fifth cycle.

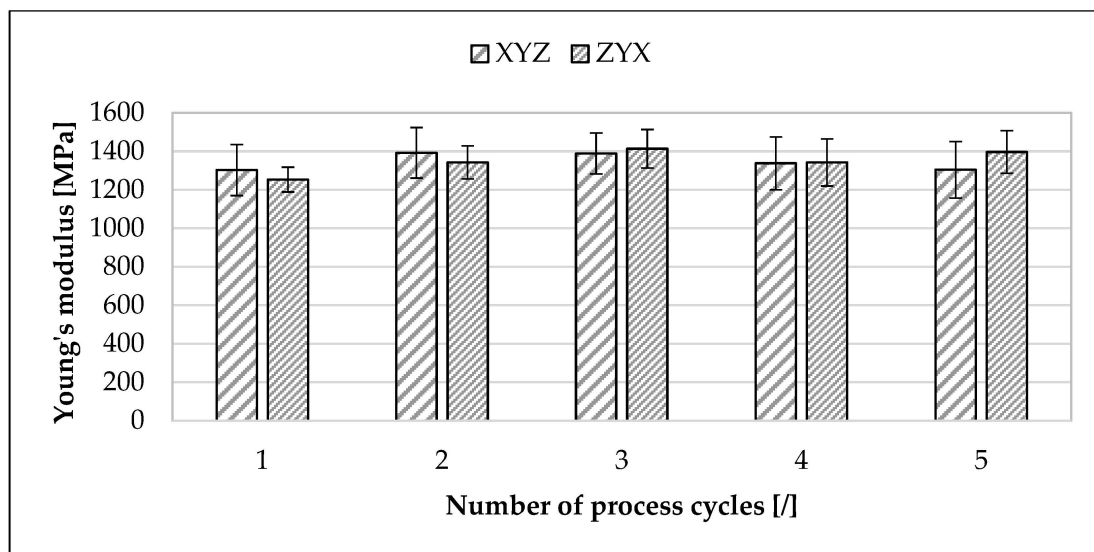
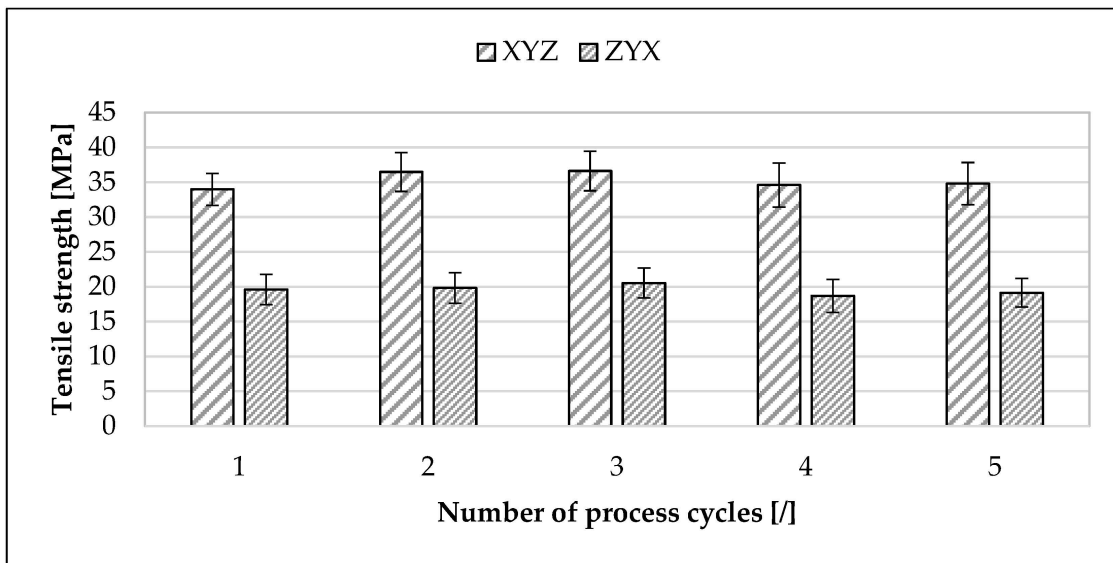


**Figure 11.** Influence of cyclic reuse on Young's modulus of the specimens manufactured from the used polyamide 12 sinter material. Five process cycles were considered. XYZ- and ZYX-specimens were analyzed. The refresh rate was 30 wt%.

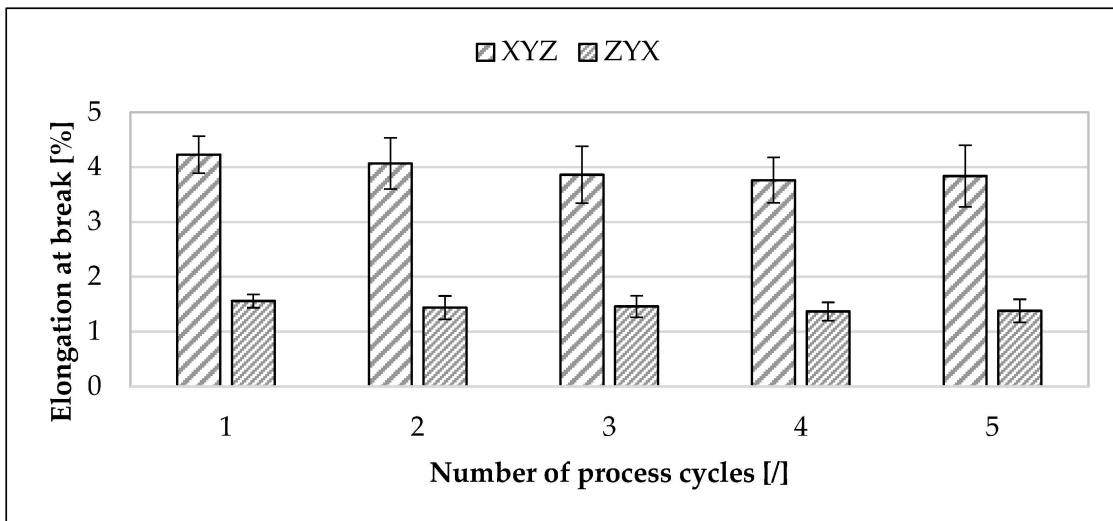
In the first cycle, Young's modulus for the XYZ-specimens (1302.45 MPa) was approx. 3.8% higher than Young's modulus for the ZYX-specimens (1253.00 MPa). In the fifth cycle, Young's modulus for the XYZ-specimens (1304.04 MPa) was about 7% lower than Young's modulus for the ZYX-specimens (1396.52 MPa).

Figure 12 illustrates the influence of cyclic reuse on tensile strength. The tensile strength of the XYZ- and ZYX-specimens each decreased by approx. 2.5% within five process cycles. In the first cycle, the tensile strength of the XYZ-specimens (33.97 MPa) was approx. 42.3% higher than the tensile strength of the ZYX-specimens (19.60 MPa). In the fifth cycle, the tensile strength of the XYZ-specimens (34.80 MPa) was approx. 45% higher than the tensile strength of the ZYX-specimens (19.13 MPa).

Figure 13 illustrates the influence of cyclic reuse on the elongation at break. The elongation at the break of the XYZ-specimens decreased from the first to the fifth cycle from 4.23 to 3.84%. In addition, the elongation at the break of the ZYX-specimens decreased in the same number of process cycles from 1.56% to 1.38%. During the cyclic reuse, the ratio of elongation at the break of the XYZ-specimens to the ZYX-specimens remained constant at approx. 63.5%.



**Figure 12.** Influence of cyclic reuse on tensile strength of the specimens manufactured from the used polyamide 12 sinter material. Five process cycles were considered. XYZ- and ZYX-specimens were analyzed. The refresh rate was 30 wt%.



**Figure 13.** Influence of cyclic reuse on elongation at the break of the specimens manufactured from the used polyamide 12 sinter material. Five process cycles were considered. XYZ- and ZYX-specimens were analyzed. The refresh rate was 30 wt%.

### 3.2.2. Sinter Density

Figure 14 illustrates the influence of cyclic reuse on sinter density. From the first to the fifth process cycle, there was an increase in sinter density of approx. 0.4%. The change in sinter density was within the standard deviation. Only the second cycle showed an increase in sinter density of approx. 4% compared to the first cycle. Regarding the first cycle, the standard deviation and variation coefficient increased with continuous reuse. The variation coefficient increased by approx. 3% from the first to the last cycle.

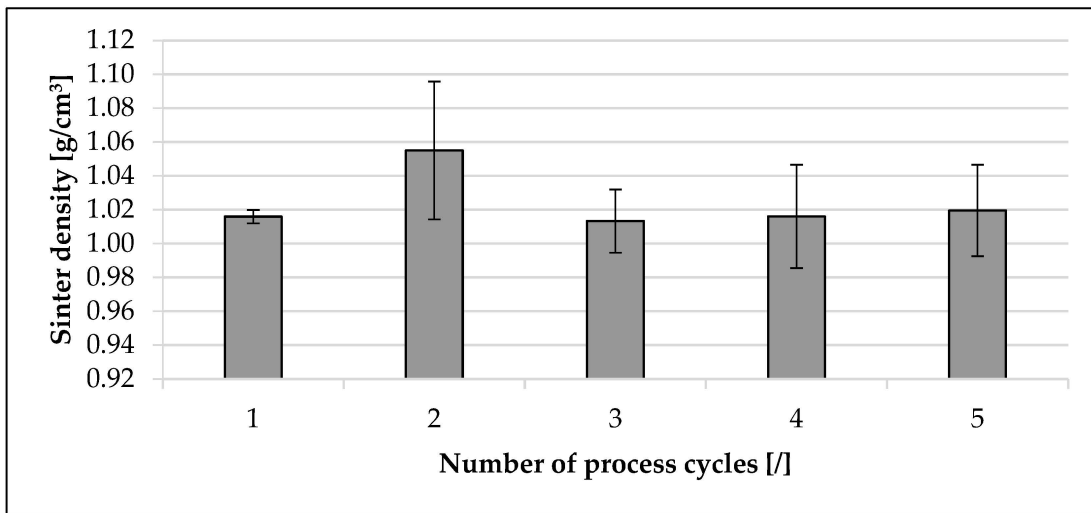


**Figure 14.** Influence of cyclic reuse on sinter density. Five process cycles were considered. The refresh rate was 30 wt%.

3.2.3. Surface Roughness

Figure 15 illustrates the influence of cyclic reuse on surface roughness ( $S_a$ ). The downskin surfaces of all the process cycles had a lower surface roughness than the upskin and sideskin surfaces. In relation to the first process cycle, the surface roughness of the upskin surface was approx. 14.3% higher than the surface roughness of the downskin surface and was approx. 24.5% lower than the surface roughness of the sideskin surface. Within five process cycles, the surface roughness of the upskin surface increased by approx. 9.5%. In addition, the surface roughness of the sideskin surface increased by approx. 11% and the surface roughness of the downskin surface increased by approx. 10.6%.

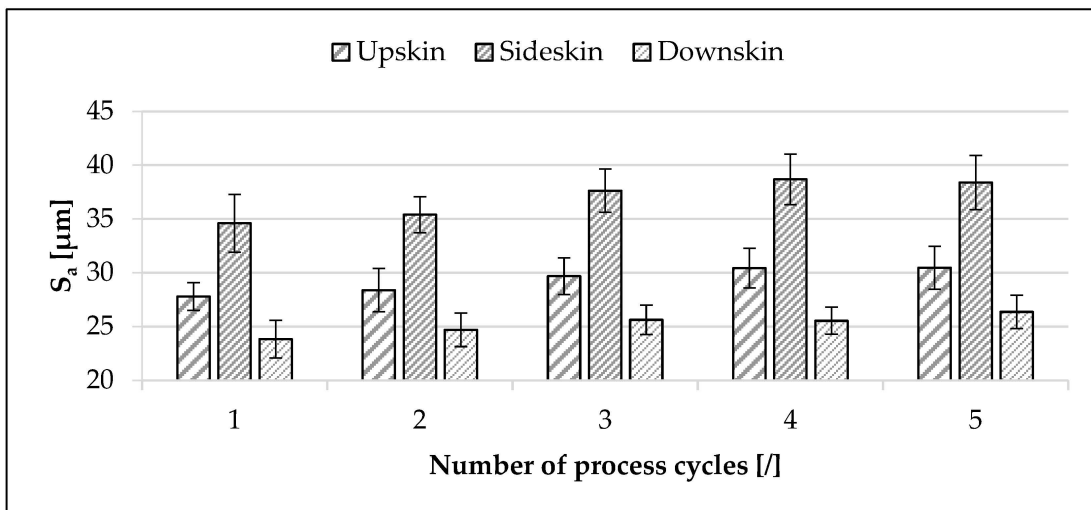


**Figure 15.** Influence of cyclic reuse on surface roughness ( $S_a$ ) of the specimens manufactured from the used polyamide 12 sinter material. Five process cycles were considered. The upskin, sideskin, and downskin-surfaces were analyzed. The refresh rate was 30 wt%.

The  $S_z$ -value (Figure 16) behaved analogously to the  $S_a$ -value. In relation to the first process cycle, the surface roughness of the upskin surface was approx. 17.4% higher than the surface roughness of the downskin surface, and approx. 15.8% lower than the surface roughness of the sideskin surface. Due to the cyclic reuse in process cycles, the surface roughness of the upskin surface increased by approx. 10.2%. In addition, the surface

roughness of the sideskin surface increased by approx. 12.8% and the surface roughness of the downskin surface increased by approx. 2.4%.

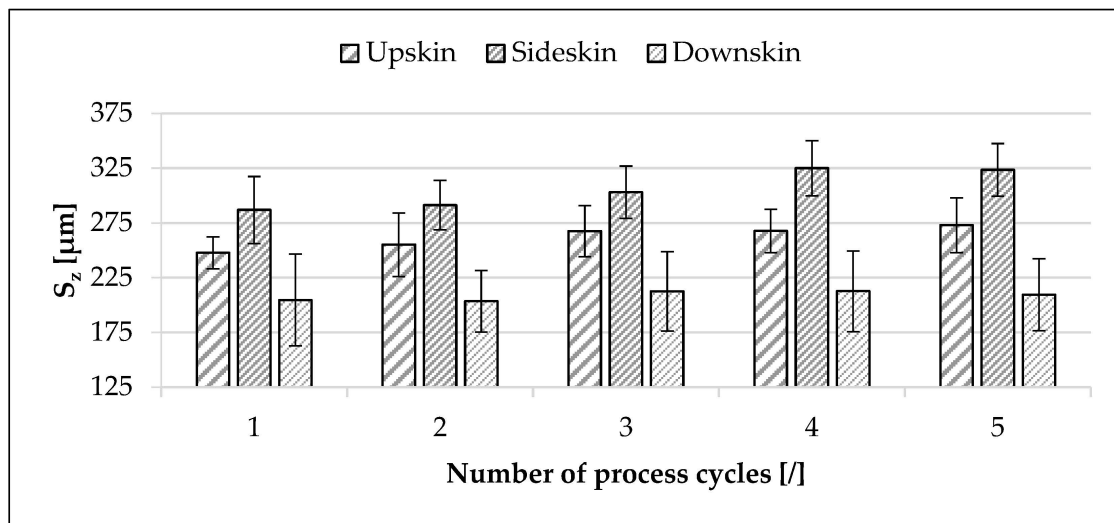


**Figure 16.** Influence of cyclic reuse on surface roughness ( $S_z$ ) of the specimens manufactured from the used polyamide 12 sinter material. Five process cycles were considered. The upskin, sideskin, and downskin surfaces were analyzed. The refresh rate was 30 wt%.

### 3.2.4. Discussion of the Results of the Studies on Component Properties

Basically, the occurrence of specific aging mechanisms can be assumed to depend on the used SLS system and the selected process parameters [69,70]. By avoiding inert gases in the SLS system, an additional change in the chemical properties of the material and the particle properties as a result of the presence of high temperatures and reactive gases can be ruled out [1]. Contrary to previous studies [1,6,19,22–24,70,75,81,84,87], which indicate a decrease in the mechanical properties with an increasing number of process cycles, this work shows that Young's modulus for the ZYX-specimens, in particular, increased with the increasing degree of reuse (Figure 11). The reason for the deviating results could be overlapping effects due to the constant refreshing with new powder as well as a too-low number of investigated process cycles. Furthermore, it should be noted that the changes in Young's modulus were within the corresponding standard deviation and thus there was no clearly measurable influence of the cyclic reuse. The isotropic appearance of Young's modulus was due to the measurement method. Here, Young's modulus was recorded in a deformation interval in which the anisotropic behavior of the specimens was not already apparent in the result [5,45].

In addition, the decrease in tensile strength of the XYZ- and ZYX-specimens with the increasing number of process cycles as shown in Figure 12 has been confirmed by previous studies [1,6,19,22–24,70,75,81,84,87]. The reason for this could be a decreasing degree of crystallinity with an increasing degree of reuse, whereby the intermolecular interactions and the mobility of the lamellar structure decrease under mechanical load. As a result, the tensile strength decreases [6,88]. Moreover, the observed increase in particle size (Figure 5) and decrease in powder density (Figures 7 and 8) could also have favored the recorded decrease in tensile strength. These phenomena could result in defects within the material and notch effects on the component surface [1,5]. The investigations showed a clear anisotropy of the specimens [1,5], with ZYX-specimens showing a lower tensile strength (Figure 12) and elongation at break (Figure 13) than XYZ-specimens. The decrease of the cyclic reuse on the elongation at the break of the specific specimens, recorded in Figure 13, has been confirmed by Dadbakhsh et al. [6]. According to the results presented here, the material behavior becomes increasingly brittle with an increasing number of process cycles. This finding is in contrast to the increase in ductility recorded in studies [65,81,86]. A possible increase in the elongation at break due to spherulite growth did not occur. It is

possible that the decrease in the elongation at break resulted in a weakened component bond and a lower coalescence of the material. However, this assumption was not confirmed by the MFR value recorded in Figure 10. The constant and low standard deviation recorded in Figures 11–13 indicates a homogeneous mixing of the powder fractions and a suitable choice of mixing parameters.

Contrary to the findings of Alscher [82], no influence of cyclic reuse on sinter density was recorded (Figure 14). One reason for this could be that the expected increase in melt viscosity, which makes permeation of the molten phase more difficult, was not recorded (Figure 10). The increase in the variation coefficient from the first to the further cycles could be the first sign of the influence of aging. The refreshing with new powder possibly overrode the material aging effects. In addition, the number of investigated process cycles may not have been sufficient to detect such effects mentioned in Alscher [82]. The slight change in the variation coefficient from the first to the last cycle of less than 5% indicates a homogeneous mixing of the powder fractions.

Although no increase in molecular weight was observed (Figure 10), an increase in surface roughness due to cyclic reuse was observed (Figure 16), which is confirmed by various studies [22,70,71,84]. Contrary to previous studies [1,61,62,89], the downskin surface had the lowest surface roughness (Figure 16). In accordance with these studies, the sideskin surface had the highest surface roughness. The reason for these results could be the use of SLS equipment and process parameters, as well as the sinter material, so that a flat powder surface was not already present during the powder application process [69,70]. Another possibility is that the dwell time of the powder application was too short. As a result, the upskin surface was not completely solidified when the next powder layer was applied and the powder particles were embedded in the component surface. These particles consequently influenced the surface roughness.

#### 4. Conclusions and Outlook

In order to ensure gentle and homogeneous mixing of the powder fractions, and thus to compensate for the influence of aging on the material and component properties, mixing parameters were already determined in a previous part of the study [31] for the polyamide 12 sinter material and mixing technique used in this work. The aim of this work was to investigate the influence of these mixing parameters on the powder and component properties during continuous processing in the SLS at a constant refresh rate. The focus of the investigation was on the thermal and rheological behavior, particle characteristics, and density of the powder, as well as on the mechanical properties, sinter density, and surface quality of the resulting components. The main conclusions are summarized as follows:

- The particle size increased up to 22% (D10-value);
- The bulk density of the powder decreased up to 6.5%. The gap between the density of printing and aged powder increased with the increasing number of cycles;
- The refresh rate of 30 wt% ensured that the form factors, the density of the printing powders, and the sinter window were maintained;
- The MFR value decreased by approx. 9.7%;
- Depending on the specimen orientation, the tensile strength decreased up to 2.5%, and the elongation at break up to 11.5%. No influence Young's modulus;
- No direct influence on sinter density was recorded. The variation coefficient of the sinter density increased by a maximum of 3%;
- The downskin surface had the lowest surface roughness, followed by the upskin and sideskin surface. The surface roughness for the analyzed surfaces increased up to 11% with the increasing number of process cycles;
- The selected mixing parameters of 1 h and 15 rpm ensured a gentle and homogeneous mixing of the powder fractions.

Although the investigations carried out in the previous part [31] and this part of the study ensured that the powder fractions were mixed homogeneously and in a manner that was gentle on the material, this work created scope for further investigations. In addition

to the analysis of bulk and tap density, other investigation methods for the analysis of powder flow could also be considered. Various possibilities for determining the powder flow are mentioned in Schulze [9]. The powder reuse technique applied in this study was helpful for the cyclic application of SLS for reproducible and high-quality polymer processing. This part of the study can be used to understand how the ongoing powder and component properties of the used polyamide 12 sinter material change during cyclic reuse. Furthermore, this study confirmed that the selected mixing parameters allowed a homogeneous and gentle mixing of the powder fractions even in the case of cyclic use of the material. Even though an influence trend of the cyclic reuse can be recognized for almost all investigated powder and component properties, the results of this work will be verified by the analysis of further process cycles, and abort criteria of cyclic use can be selected to achieve an acceptable and reproducible component quality. Regarding the influence of cyclic reuse on the powder and component properties, it is evident that the refresh rate overlays possible ageing effects.

The results of this study are generally valid for the chosen polyamide 12 sinter material and methods. Therefore using a different SLS setup, sinter material, mixing technique, and mixing parameters, as well as different testing methods, may show deviations from the obtained results. However, comparable trends in results can be expected when using other sinter materials, as the polymer sinter materials are exposed to various material aging processes during SLS [1,19–24]. The degree of material aging and its effects on material and component properties may conceivably depend on the used sinter material. The application of the investigation to other materials and SLS systems is a task of future studies. In future studies, the influence of the refresh rate could be considered as an additional parameter. Furthermore, the influence of cyclic reuse on the characteristics and degradation of stabilizers and additives in the powder [5], as well as on the triboelectric properties of the powder [17,68], should be investigated.

**Author Contributions:** Conceptualization, T.E. and F.v.L.; methodology, T.E.; validation, T.E. and F.v.L.; formal analysis, T.E.; investigation, T.E.; resources, T.E. and F.v.L.; data curation, T.E.; writing—original draft preparation, T.E.; writing—review and editing, T.E. and F.v.L.; visualization, T.E.; supervision, F.v.L.; project administration, T.E. and F.v.L. All authors have read and agreed to the published version of the manuscript.

**Funding:** This research received no external funding.

**Data Availability Statement:** The raw/processed data required to reproduce these findings cannot be shared at this time as the data also form part of an ongoing study.

**Conflicts of Interest:** The authors declare no conflict of interest. The results, opinions, and conclusions expressed in this publication are not necessarily those of Volkswagen Aktiengesellschaft.

## References

1. Gibson, I.; Rosen, D.; Stucker, B. *Additive Manufacturing Technologies: 3D Printing, Rapid Prototyping and Direct Digital Manufacturing*, 2nd ed.; Springer: New York, NY, USA; Berlin/Heidelberg, Germany; Dordrecht, The Netherlands; London, UK, 2015; ISBN 978-1-4939-2112-6.
2. Celik, E. *Additive Manufacturing*; De Gruyter: Berlin, Germany, 2020; ISBN 9781501518782.
3. Seppala, J.E.; Kotula, A.P.; Snyder, C.R. *Polymer-Based Additive Manufacturing: Recent Developments*; American Chemical Society: Washington, DC, USA, 2019; ISBN 9780841234260.
4. Goodridge, R.D.; Tuck, C.J.; Hague, R. Laser sintering of polyamides and other polymers. *Prog. Mater. Sci.* **2012**, *57*, 229–267. [[CrossRef](#)]
5. Schmid, M. *Selektives Lasersintern (SLS) mit Kunststoffen: Technologie, Prozesse und Werkstoffe*; Hanser: München, Germany, 2015; ISBN 978-3-446-44562-8.
6. Dadbakhsh, S.; Verbelen, L.; Verkinderen, O.; Strobbe, D.; van Puyvelde, P.; Kruth, J.-P. Effect of PA12 powder reuse on coalescence behaviour and microstructure of SLS parts. *Eur. Polym. J.* **2017**, *92*, 250–262. [[CrossRef](#)]
7. Schmid, M.; Amado, A.; Wegener, K. Polymer powders for selective laser sintering (SLS). In Proceedings of the PPS-30: The 30th International Conference of the Polymer Processing Society—Conference Papers, Cleveland, OH, USA, 6–12 June 2014; AIP Publishing LLC: Melville, NY, USA, 2015; p. 160009.

8. Schmid, M.; Wegener, K. Additive Manufacturing: Polymers Applicable for Laser Sintering (LS). *Procedia Eng.* **2016**, *149*, 457–464. [[CrossRef](#)]
9. Schulze, D. *Pulver und Schüttgüter*; Springer: Berlin/Heidelberg, Germany, 2019; ISBN 978-3-662-58775-1.
10. Schatt, W.; Kieback, B.; Wieters, K.-P. (Eds.) *Pulvermetallurgie: Technologien und Werkstoffe*, 2nd ed.; Bearbeitete und Erweiterte Auflage; Springer: Berlin/Heidelberg, Germany, 2007; ISBN 978-3-540-23652-8.
11. Masuda, H.; Higashitani, K.; Yoshida, H. *Powder Technology: Fundamentals of Particles, Powder Beds, and Particle*; CRC Press: Boca Raton, FL, USA, 2019; ISBN 9780367389802.
12. Mys, N.; Verberckmoes, A.; Cardon, L. Expanding the material palette for Selective Laser Sintering: Two production techniques for spherical powders. In Proceedings of the PMI 2018: 8th Bi-Annual International Conference on Polymers and Moulds Innovations, Guimaraes, Portugal, 19–21 September 2018; Pontes, A., Ed.; Institute of Polymers and Composites, University of Minho: Braga, Portugal, 2018; p. 7, ISBN 9789892088099.
13. Hirschberg, C.; Sun, C.C.; Risbo, J.; Rantanen, J. Effects of Water on Powder Flowability of Diverse Powders Assessed by Complimentary Techniques. *J. Pharm. Sci.* **2019**, *108*, 2613–2620. [[CrossRef](#)] [[PubMed](#)]
14. Faqih, A.M.N.; Mehrotra, A.; Hammond, S.V.; Muzzio, F.J. Effect of moisture and magnesium stearate concentration on flow properties of cohesive granular materials. *Int. J. Pharm.* **2007**, *336*, 338–345. [[CrossRef](#)] [[PubMed](#)]
15. Drummer, D.; Wudy, K.; Drexler, M. Influence of energy input on degradation behavior of plastic components manufactured by selective laser melting. *Phys. Procedia* **2014**, *56*, 176–183. [[CrossRef](#)]
16. Berretta, S.; Ghita, O.; Evans, K.E. Morphology of polymeric powders in Laser Sintering (LS): From Polyamide to new PEEK powders. *Eur. Polym. J.* **2014**, *59*, 218–229. [[CrossRef](#)]
17. Hesse, N.; Dechet, M.A.; Bonilla, J.S.G.; Lübbert, C.; Roth, S.; Bück, A.; Schmidt, J.; Peukert, W. Analysis of tribo-charging during powder spreading in Selective Laser Sintering: Assessment of polyamide 12 powder ageing effects on charging behavior. *Polymers* **2019**, *11*, 609. [[CrossRef](#)]
18. Amado, A.; Schmid, M.; Levy, G.; Wegener, K. Advances in SLS powder characterization. In Proceedings of the 22nd Annual International Solid Freeform Fabrication Symposium—An Additive Manufacturing Conference, SFF 2011, Austin, TX, USA, 8–10 August 2011.
19. Choren, J.; Gervasi, V.; Herman, T.; Kamara, S.; Mitchell, J. SLS powder life study. In Proceedings of the 2001 Solid Freeform Fabrication Symposium, Austin, TX, USA, 6–8 August 2001; pp. 39–45.
20. Dahlmann, R.; Haberstroh, E.; Menges, G. *Menges Werkstoffkunde Kunststoffe, Vollständig neu Bearbeitete Auflage*, 7th ed.; Hanser: Munich, Germany, 2022; ISBN 978-3-446-45801-7.
21. *DIN 50035:2012-09; Begriffe auf dem Gebiet der Alterung von Materialien—Polymere Werkstoffe*. Beuth Verlag GmbH: Berlin, Germany, 2012.
22. Dotchev, K.; Yusoff, W. Recycling of polyamide 12 based powders in the laser sintering process. *Rapid Prototyp. J.* **2009**, *15*, 192–203. [[CrossRef](#)]
23. Drummer, D.; Harder, R.G.; Witt, G.; Wegner, A.; Wudy, K.; Drexler, M. Long-term Properties of Laser Sintered Parts of Polyamide 12—Influence of Storage Time and Temperature on the Aging Behavior. *Int. J. Recent Contrib. Eng. Sci. IT* **2015**, *3*, 20–27. [[CrossRef](#)]
24. Kühnlein, F.; Drummer, D.; Rietzel, D.; Seefried, A. Degradation behavior and material properties of PA 12 plastic powders processed by powder based additive manufacturing technologies. In Proceedings of the Annals of DAAAM for 2010 & Proceedings of the 21st International DAAAM Symposium, Zadar, Croatia, 20–23 October 2010; DAAAM International Vienna: Vienna, Austria, 2010; Volume 21, pp. 1–2.
25. Fiedler, L.; Androsch, R.; Mileva, D.; Radosch, H.J.; Wutzler, A.; Gerken, J. Experimentelle Simulation der physikalischen Alterung von Lasersinterpulvern. *Z. Kunstst.* **2010**, *6*, 19–32.
26. Josupeit, S.; Lohn, J.; Hermann, E.; Gessler, M.; Tenbrink, S.; Schmid, H.-J. Material Properties of Laser Sintered Polyamide 12 as Function of Build Cycles Using Low Refresh Rates. In Proceedings of the 26th Annual International Solid Freeform Fabrication Symposium, Austin, TX, USA, 10–12 August 2015; pp. 540–549.
27. Wudy, K.; Drummer, D.; Kühnlein, F.; Drexler, M. Influence of degradation behavior of polyamide 12 powders in laser sintering process on produced parts. In Proceedings of the PPS-29: The 29th International Conference of the Polymer Processing Society—Conference Papers, Nuremberg, Germany, 15–19 July 2013; American Institute of Physics: College Park, MD, USA, 2014; pp. 691–695.
28. Breuninger, J.; Becker, R.; Wolf, A.; Rommel, S.; Verl, A. *Generative Fertigung mit Kunststoffen: Konzeption und Konstruktion für Selektives Lasersintern*; Springer: Berlin/Heidelberg, Germany, 2013; ISBN 978-3-642-24324-0.
29. Gebhardt, A. *Additive Fertigungsverfahren: Additive Manufacturing und 3D-Drucken für Prototyping—Tooling—Produktion*, 5th ed.; neu bearbeitete und erweiterte Auflage; Hanser: München, Germany, 2016; ISBN 978-3-446-44401-0.
30. Mielicki, C. Prozessnahes Qualitätsmanagement beim Lasersintern von Polyamid 12. Ph.D. Thesis, Universität Duisburg-Essen, Duisburg, Germany, Essen, Germany, 2014.
31. Eggers, T.; Rackl, H.; von Lacroix, F. Investigation of the Influence of the Mixing Process on the Powder Characteristics for Cyclic Reuse in Selective Laser Sintering. *Powders* **2023**, *2*, 32–46. [[CrossRef](#)]
32. Lehmann&Voss&Co. KG. *LUVOSINT PA12 9270 BK—Polyamide 12 Unreinforced, Black: Preliminary Datasheet*; Lehmann&Voss&Co.: Hamburg, Germany, 2022.

33. DIN EN ISO 527-2:2012-06; Kunststoffe-Bestimmung der Zugeigenschaften-Teil\_2: Prüfbedingungen für Form- und Extrusionsmassen (ISO\_527-2:2012). Deutsche Fassung EN\_ISO\_527-2:2012. Beuth Verlag GmbH: Berlin, Germany, 2012.
34. DIN ISO 3310-1:2017-11; Analysensiebe-Technische Anforderungen und Prüfung-Teil\_1: Analysensiebe mit Metalldrahtgewebe (ISO\_3310-1:2016). Beuth Verlag GmbH: Berlin, Germany, 2017.
35. Weber, S. Untersuchungen zum Einfluss der Mischintensität auf die Potenz Nanostrukturierter Fließregulierungsmittel. Ph.D. Thesis, Julius-Maximilians-Universität Würzburg, Würzburg, Germany, 2009.
36. Stieß, M. *Mechanische Verfahrenstechnik—Partikeltechnologie 1*, 3rd ed.; Vollst. Neu Bearb; Springer: Berlin/Heidelberg, Germany, 2009; ISBN 978-3-540-32551-2.
37. Weinekötter, R.; Gericke, H. *Mischen von Feststoffen: Prinzipien, Verfahren, Mischer*; Springer: Berlin/Heidelberg, Germany, 1995; ISBN 978-3-540-58567-1.
38. Sommer, K. Mechanismen des Pulvermischens. *Chem. Ing. Tech.* **1977**, *49*, 305–311. [[CrossRef](#)]
39. Jonat, S.; Hasenzahl, S.; Drechsler, M.; Albers, P.; Wagner, K.; Schmidt, P. Investigation of compacted hydrophilic and hydrophobic colloidal silicon dioxides as glidants for pharmaceutical excipients. *Powder Technol.* **2004**, *141*, 31–43. [[CrossRef](#)]
40. Bhoite, K.; Kakandikar, G.M.; Nandedkar, V.M. Schatz Mechanism with 3D-Motion Mixer-A Review. *Mater. Today Proc.* **2015**, *2*, 1700–1706. [[CrossRef](#)]
41. Blümel, C. *Charakterisierung der Trocken Beschichtung zur Herstellung von Maßgeschneiderten Kompositpartikeln*; Universität Erlangen-Nürnberg: Erlangen, Germany, 2015; ISBN 978-3-8439-2120-6.
42. Mwania, F.M.; Maringa, M.; van der Walt, K. Mixing and Reuse of Polymer Laser Sintering Powders to Ensure Homogeneity—A Review. *Int. J. Eng. Res. Technol.* **2020**, *13*, 3335. [[CrossRef](#)]
43. ISO 13322-2:2021-12; Particle Size Analysis—Image Analysis Methods—Part 2: Dynamic Image Analysis Methods. International Organization of Standardization: Vernier, Switzerland; Geneva, Switzerland, 2021.
44. Wadell, H. Volume, Shape, and Roundness of Quartz Particles. *J. Geol.* **1935**, *43*, 250–280. [[CrossRef](#)]
45. Frick, A.; Stern, C. *Einführung in die Kunststoffprüfung: Prüfmethoden und Anwendungen*; Hanser: München, Germany, 2017; ISBN 978-3-446-44351-8.
46. Carr, J.F.; Walker, D.M. An annular shear cell for granular materials. *Powder Technol.* **1968**, *1*, 369–373. [[CrossRef](#)]
47. Carr, R.L., Jr. Evaluating flow properties of solids. *Chem. Eng.* **1965**, *18*, 163–168.
48. Spierings, A.B.; Voegtlin, M.; Bauer, T.; Wegener, K. Powder flowability characterisation methodology for powder-bed-based metal additive manufacturing. *Prog. Addit. Manuf.* **2016**, *1*, 9–20. [[CrossRef](#)]
49. Zhou, Q.; Qu, L.; Larson, I.; Stewart, P.J.; Morton, D.A. Effect of mechanical dry particle coating on the improvement of powder flowability for lactose monohydrate: A model cohesive pharmaceutical powder. *Powder Technol.* **2011**, *207*, 414–421. [[CrossRef](#)]
50. Mullarney, M.P.; Beach, L.E.; Davé, R.N.; Langdon, B.A.; Polizzi, M.; Blackwood, D.O. Applying dry powder coatings to pharmaceutical powders using a comil for improving powder flow and bulk density. *Powder Technol.* **2011**, *212*, 397–402. [[CrossRef](#)]
51. Abdullah, E.C.; Geldart, D. The use of bulk density measurements as flowability indicators. *Powder Technol.* **1999**, *102*, 151–165. [[CrossRef](#)]
52. DIN EN ISO 60:2000-01; Kunststoffe-Bestimmung der Scheinbaren Dichte von Formmassen, Die Durch Einen Genormten Trichter Abfließen Können (Schüttdichte) (ISO\_60:1977). Deutsche Fassung EN\_ISO\_60:1999. Beuth Verlag GmbH: Berlin, Germany, 2000.
53. DIN EN ISO 787-11:1995-10; Allgemeine Prüfverfahren für Pigmente und Füllstoffe-Teil\_11: Bestimmung des Stampfvolumens und der Stampfdichte (ISO\_787-11:1981). Deutsche Fassung EN\_ISO\_787-11:1995. Beuth Verlag GmbH: Berlin, Germany, 1995.
54. DIN EN ISO 1133-1:2012-03; Kunststoffe-Bestimmung der Schmelze-Massefließrate (MFR) und der Schmelze-Volumenfließrate (MVR) von Thermoplasten-Teil\_1: Allgemeines Prüfverfahren (ISO\_1133-1:2011). Deutsche Fassung EN\_ISO\_1133-1:2011. Beuth Verlag GmbH: Berlin, Germany, 2012.
55. DIN EN ISO 11357-1:2017-02; Kunststoffe-Dynamische Differenz-Thermoanalyse (DSC)-Teil\_1: Allgemeine Grundlagen (ISO\_11357-1:2016). Deutsche Fassung EN\_ISO\_11357-1:2016. Beuth Verlag GmbH: Berlin, Germany, 2017.
56. Schmid, M.; Kleijnen, R.; Vetterli, M.; Wegener, K. Influence of the Origin of Polyamide 12 Powder on the Laser Sintering Process and Laser Sintered Parts. *Appl. Sci.* **2017**, *7*, 462. [[CrossRef](#)]
57. DIN EN ISO 16396-2:2017-07; Kunststoffe-Polyamid\_(PA)-Formmassen für das Spritzgießen und die Extrusion-Teil\_2: Herstellung von Probekörpern und Bestimmung von Eigenschaften (ISO\_16396-2:2017). Deutsche Fassung EN\_ISO\_16396-2:2017. Beuth Verlag GmbH: Berlin, Germany, 2017.
58. DIN EN ISO 527-1:2019-12; Kunststoffe-Bestimmung der Zugeigenschaften-Teil\_1: Allgemeine Grundsätze (ISO\_527-1:2019). Deutsche Fassung EN\_ISO\_527-1:2019. Beuth Verlag GmbH: Berlin, Germany, 2019.
59. DIN EN ISO 4287:2010-07; Geometrische Produktspezifikation (GPS)-Oberflächenbeschaffenheit: Tastschnittverfahren-Benennungen, Definitionen und Kenngrößen der Oberflächenbeschaffenheit (ISO\_4287:1997\_+ Cor\_1:1998\_+ Cor\_2:2005\_+ Amd\_1:2009); Deutsche Fassung EN\_ISO\_4287:1998\_+ AC:2008\_+ A1:2009. Beuth Verlag GmbH: Berlin, Germany, 2010.
60. DIN EN ISO 25178-1:2016-12; Geometrische Produktspezifikation\_(GPS)-Oberflächenbeschaffenheit: Flächenhaft-Teil\_1: Angabe von Oberflächenbeschaffenheit (ISO\_25178-1:2016). Deutsche Fassung EN\_ISO\_25178-1:2016. Beuth Verlag GmbH: Berlin, Germany, 2016.
61. Thomas, D. The Development of Design Rules for Selective Laser Melting. Ph.D. Thesis, University of Wales, Cardiff, Wales, 2009.

62. Schwaneckamp, T.; Bräuer, M.; Reuber, M. Geometrical and topological potentialities and restrictions in selective laser sintering of customized carbide precision tools. In Proceedings of the Lasers in Manufacturing Conference, Munich, Germany, 26–29 June 2017; pp. 26–29.
63. Mielicki, C.; Gronhoff, B.; Wortberg, J. Effects of laser sintering processing time and temperature on changes in polyamide 12 powder particle size, shape and distribution. In Proceedings of the PPS-29: The 29th International Conference of the Polymer Processing Society—Conference Papers, Nuremberg, Germany, 15–19 July 2013; American Institute of Physics: Melville, NY, USA, 2014; pp. 728–731.
64. Seul, T. Ansätze zur Werkstoffoptimierung beim Lasersintern durch Charakterisierung und Modifizierung Grenzflächenenergetischer Phänomene: Approach for Optimizing Material for Lasersintering by Means of Characterisation and Modification interfacial-Energy-Phenomenon. Ph.D. Thesis, RWTH Aachen, Aachen, Germany, 2004.
65. Sauer, A. Optimierung der Bauteileigenschaften beim Selektiven Lasersintern von Thermoplasten. Ph.D. Thesis, Shaker, Aachen, Germany, 2005.
66. Fockele, M. Powder Processing Method. WO 2014/167100 A1, 16 October 2014.
67. Rietzel, D. Werkstoffverhalten und Prozessanalyse beim Laser-Sintern von Thermoplasten. Ph.D. Thesis, Friedrich-Alexander-Universität Erlangen-Nürnberg, Erlangen-Nürnberg, Germany, 2011.
68. Schmidt, J.; Dechet, M.A.; Gómez Bonilla, J.S.; Hesse, N.; Bück, A.; Peukert, W. Characterization of polymer powders for selective laser sintering. In Proceedings of the 2019 International Solid Freeform Fabrication Symposium, Austin, TX, USA, 12–14 August 2019; pp. 779–789.
69. Wegner, A. Theorie über die Fortführung von Aufschmelzvorgängen als Grundvoraussetzung für eine Robuste Prozessführung beim Laser-Sintern von Thermoplasten. Ph.D. Thesis, Universität Duisburg-Essen, Duisburg, Germany, Essen, Germany, 2015.
70. Wegner, A.; Mielicki, C.; Grimm, T.; Gronhoff, B.; Witt, G.; Wortberg, J. Determination of Robust Material Qualities and Processing Conditions for Laser Sintering of Polyamide 12. *Polym. Eng. Sci.* **2014**, *54*, 1540–1554. [[CrossRef](#)]
71. Pham, D.; Dotchev, K.; Yusoff, W. Deterioration of polyamide powder properties in the laser sintering process. *Proc. Inst. Mech. Eng. Part C J. Mech. Eng. Sci.* **2008**, *222*, 2163–2176. [[CrossRef](#)]
72. Kühnlein, F.; Drummer, D.; Wudy, K.; Drexler, M. Alterungsmechanismen der Kunststoffpulvern bei der Verarbeitung und deren Einfluss auf prozessrelevante Materialeigenschaften. *Ind. Sonderforschungsbereichs* **2012**, *814*, 49–66.
73. Drummer, D.; Kühnlein, F.; Rietzel, D.; Hülder, G. Untersuchung der Materialalterung bei pulverbasierten Schichtbauverfahren. In *RTEjournal-Forum für Rapid Technologie*; Aachen University of Applied Sciences: Aachen, Germany, 2010.
74. Gornet, T. Materials and process control for rapid manufacture. In *Rapid Manufacturing: An Industrial Revolution for the Digital Age*; John Wiley & Sons: Chichester, UK, 2006; pp. 125–146.
75. Gornet, T.J.; Davis, K.R.; Starr, T.L.; Mulloy, K.M. Characterization of Selective Laser Sintering™ Materials to Determine Process Stability. In Proceedings of the 2002 International Solid Freeform Fabrication Symposium, Austin, TX, USA, 5–7 August 2002; pp. 546–553.
76. Griebach, S. Korrelation Zwischen Materialzusammensetzung, Herstellungsbedingungen und Eigenschaftsprofil von Laser-gesinterten Polyamid-Werkstoffen. Ph.D Thesis, Verlag Wissenschaftliche Scripten, Auerbach, Germany, 2012.
77. Wudy, K.; Drummer, D. Aging effects of polyamide 12 in selective laser sintering: Molecular weight distribution and thermal properties. *Addit. Manuf.* **2019**, *25*, 1–9. [[CrossRef](#)]
78. Zarringhalam, H.; Hopkinson, N.; Kamperman, N.F.; Vlieger, J.J.d. Effects of processing on microstructure and properties of SLS Nylon 12. *Mater. Sci. Eng. A* **2006**, *435*, 172–180. [[CrossRef](#)]
79. Rösenberg, S.; Weiffen, R.; Knoop, F.C.; Schmid, H.-J.; de Gessler, M.; Pfisterer, H. Controlling the Quality of Laser Sintered Parts Along the Process Chain. In Proceedings of the 23rd International Solid Freeform Fabrication Symposium (SFF 2012), Austin, TX, USA, 6–8 August 2012; pp. 1024–1044.
80. Haworth, B.; Hopkinson, N.; Hitt, D.J.; Zhong, X.H. Shear viscosity measurements on Polyamide-12 polymers for laser sintering. *Rapid Prototyp. J.* **2013**, *19*, 28–36. [[CrossRef](#)]
81. Haworth, B.; Hitt, D.J.; Hopkinson, N.; Vasquez, M. Laser sintering process for polymers: Influence of molecular weight and definition of a stable sintering region. In Proceedings of the Polymer Processing Society 29th Annual Meeting PPS-29, Nuremberg, Germany, 15–19 July 2013; Polymer Processing Society: Melville, N.Y, USA, 2013.
82. Alscher, G. Das Verhalten Teilkristalliner Thermoplaste beim Lasersintern. Ph.D. Thesis, Shaker, Aachen, Germany, 2000.
83. Drummer, D.; Kühnlein, F.; Rietzel, D.; Hülder, G. *Untersuchungen zum Alterungsverhalten von PA12-Kunststoffpulvern. Rapid*; Tech Proceedings: Erfurt, Germany, 2010.
84. Wegner, A.; Witt, G. Betrachtung zur Pulvernutzungsdauer beim Laser-Sintern und Einfluss der Prozessführung auf die Entstehung von Ausschussbauteilen. In *RTEjournal—Forum für Rapid Technologie*; Aachen University of Applied Sciences: Aachen, Germany, 2012.
85. Rösenberg, S.; Schmid, H.-J. Advanced characterization method of nylon 12 materials for application in laser sinter processing. In Proceedings of the PPS-29: The 29th International Conference of the Polymer Processing Society—Conference Papers, Nuremberg, Germany, 15–19 July 2013; American Institute of Physics: Melville, NY, USA, 2014; pp. 713–718.
86. Ehrenstein, G.W. *Polymer-Werkstoffe: Struktur—Eigenschaften—Anwendung*, 2nd ed.; Völlig Überarb Aufl.; Hanser: München, Germany, 1999; ISBN 9783446211612.
87. Moalli, J. (Ed.) *Plastics Failure: Analysis and Prevention*; Plastics Design Library: Norwich, NY, USA, 2010; ISBN 9781884207921.

- 
88. Magill, J.H. Review Spherulites: A personal perspective. *J. Mater. Sci.* **2001**, *36*, 3143–3164. [[CrossRef](#)]
89. Dahmen, T.; Klingaa, C.G.; Baier-Stegmaier, S.; Lapina, A.; Pedersen, D.B.; Hattel, J.H. Characterization of channels made by laser powder bed fusion and binder jetting using X-ray CT and image analysis. *Addit. Manuf.* **2020**, *36*, 101445. [[CrossRef](#)]

**Disclaimer/Publisher’s Note:** The statements, opinions and data contained in all publications are solely those of the individual author(s) and contributor(s) and not of MDPI and/or the editor(s). MDPI and/or the editor(s) disclaim responsibility for any injury to people or property resulting from any ideas, methods, instructions or products referred to in the content.